Clinical Cancer Research

Alterations in Pericyte Subpopulations Are Associated with Elevated Blood–Tumor Barrier Permeability in Experimental Brain Metastasis of Breast Cancer

L. Tiffany Lyle[1], Paul R. Lockman[2], Chris E. Adkins[2], Afroz Shareef Mohammad[2], Emily Sechrest[2], Emily Hua[1], Diane Palmieri[1], David J. Liewehr[3], Seth M. Steinberg[3], Wojciech Kloc[4,5], Ewa Izycka-Swieszewska[6,7], Renata Duchnowska[8], Naema Nayyar[9], Priscilla K. Brastianos[9], Patricia S. Steeg[1], and Brunilde Gril[1]

Abstract

Purpose: The blood–brain barrier (BBB) is modified to a blood–tumor barrier (BTB) as a brain metastasis develops from breast or other cancers. We (i) quantified the permeability of experimental brain metastases, (ii) determined the composition of the BTB, and (iii) identified which elements of the BTB distinguished metastases of lower permeability from those with higher permeability.

Experimental Design: A SUM190-BR3 experimental inflammatory breast cancer brain metastasis subline was established. Experimental brain metastases from this model system and two previously reported models (triple-negative MDA-231-BR6, HER2$^+$ JIMT-1-BR3) were serially sectioned; low- and high-permeability lesions were identified with systemic 3-kDa Texas Red dextran dye. Adjoining sections were used for quantitative immunofluorescence to known BBB and neuroinflammatory components. One-sample comparisons against a hypothesized value of one were performed with the Wilcoxon signed-rank test.

Results: When uninvolved brain was compared with any brain metastasis, alterations in endothelial, pericytic, astrocytic, and microglial components were observed. When metastases with relatively low and high permeability were compared, increased expression of a desmin$^+$ subpopulation of pericytes was associated with higher permeability (231-BR6 $P = 0.0002$; JIMT-1-BR3 $P = 0.004$; SUM190-BR3 $P = 0.008$); desmin$^+$ pericytes were also identified in human craniotomy specimens. Trends of reduced CD13$^+$ pericytes (231-BR6 $P = 0.014$; JIMT-1-BR3 $P = 0.002$, SUM190-BR3, NS) and laminin α2 (231-BR6 $P = 0.001$; JIMT-1-BR3 $P = 0.049$; SUM190-BR3 $P = 0.023$) were also observed with increased permeability.

Conclusions: We provide the first account of the composition of the BTB in experimental brain metastasis. Desmin$^+$ pericytes and laminin α2 are potential targets for the development of novel approaches to increase chemotherapeutic efficacy. *Clin Cancer Res; 22(21); 5287–99. ©2016 AACR.*

Introduction

Brain metastases of breast cancer appear to be increasing in incidence, affecting 37% of patients with metastatic HER2$^+$ breast cancer (1) and a similar percentage of patients with triple-negative tumors (estrogen and progesterone receptor–negative, HER2 normal; ref. 2). In the HER2$^+$ setting, brain metastases are commonly an early site of progression in metastatic therapy and are often serious complications in otherwise stable patients (1, 3). For patients with triple-negative tumors, brain metastases often occur in a setting of uncontrolled systemic disease (4).

One of the central questions in the brain metastasis field is the extent of breakdown of the blood–brain barrier (BBB), the protective lining of blood vessels in the brain, to form a blood–tumor barrier (BTB). An argument can be made that the BBB is compromised once a metastasis forms in the brain, as they are diagnosed by imaging gadolinium uptake. Injection of Evans Blue dye into mice harboring experimental brain metastases turned these lesions variably blue (5). Other evidence contradicts this conclusion: chemotherapy is almost completely ineffective for brain metastases (4). This is likely multifactorial, involving

[1]Women's Malignancies Branch, Center for Cancer Research, NCI, Bethesda, Maryland. [2]Department of Basic Pharmaceutical Sciences, West Virginia University Health Sciences Center, Morgantown, West Virginia. [3]Biostatistics and Data Management Section, Center for Cancer Research, NCI, Bethesda, Maryland. [4]Departments of Neurology & Neurosurgery, University of Varmia & Masuria University, Olsztyn, Poland. [5]Department of Neurosurgery, Copernicus Hospital Gdańsk, Poland. [6]Departments of Pathology & Neuropathology, Medical University of Gdańsk, Poland. [7]Department of Pathomorphology, Copernicus Hospital, Gdańsk, Poland. [8]Department of Oncology, Military Institute of Medicine, Warsaw, Poland. [9]Division of Neuro-Oncology, Massachusetts General Hospital Cancer Center, Harvard Medical School, Boston, Massachusetts.

Note: Supplementary data for this article are available at Clinical Cancer Research Online (http://clincancerres.aacrjournals.org/).

Current address for D. Palmieri: Center for Research Strategy, NCI, NIH, Bethesda, MD 20892. Current address for L. T. Lyle: Department of Comparative Pathobiology, Purdue University College of Veterinary Medicine, West Lafayette, IN 47906.

Corresponding Author: Brunilde Gril, National Cancer Institute, 37/1126 NIH, Bethesda, MD 20892. Phone: 301-451-6445; Fax: 301-402-8910; E-mail: grilbrun@mail.nih.gov

doi: 10.1158/1078-0432.CCR-15-1836

Translational Relevance

The blood–brain barrier (BBB) is modified to a blood–tumor barrier (BTB) as a brain metastasis forms from breast and other cancers. Pharmacokinetic studies indicate that the BTB is partially "open" but remains a potent obstacle to chemotherapeutic efficacy. Here, we have used quantitative immunofluorescence to characterize the BTB in three models of experimental breast cancer metastasis to the brain. Specifically, we asked what alteration(s) was associated with the highest levels of BTB permeability. High BTB permeability was associated with an increase in the desmin$^+$ pericyte subpopulation; desmin$^+$ pericytes were also identified in human craniotomy specimens. Decreases in astrocytic basement membrane component laminin α2 and the CD13$^+$ pericyte subpopulation were observed. The data provide the first account of the BTB composition in experimental brain metastasis. These alterations provide testable hypotheses for the development of new targeted therapeutic strategies to increase chemotherapeutic delivery to brain metastatic lesions.

molecular alterations in tumor cells (6) and the integrity of the BTB. In our own studies using two hematogenous experimental models of triple-negative breast cancer, heterogeneous and low levels of metastasis permeability to dyes, α-aminoisobutyric acid (AIB), and drugs were observed, that was not correlated with lesion size (7). When compared with systemic metastases, uptake was approximately a log lower in brain lesions (7, 8). The heterogeneity and overall poor permeability of the BTB permeability was confirmed using an MRI approach (9). Heterogeneous drug uptake was observed in brain metastases in a human presurgical study (10). Likely, both answers are correct: brain metastases are generally more permeable than the normal brain, but not sufficiently or homogeneously permeable to make drug therapy effective. The differences between the BBB and BTB in brain metastases are unknown. For the BTB, the distinctions between lesions that are highly permeable and poorly permeable are also unknown. These questions can only be systematically answered using animal models.

The BBB is a multicellular vascular unit that separates the central nervous system (CNS) from the peripheral blood circulation (11). Endothelial cells, astrocytes, pericytes, and two basement membranes provide both structural and functional support to the BBB. Cerebral endothelial cells constitute the inner surface and core of the BBB, characterized by a lack of fenestrae, continuous tight junctions, low pinocytotic/transcytosis activity, low levels of leukocyte adhesion molecules, and efflux pump expression (11, 12). Pericytes are mural cells involved in the stabilization of small vessels and neovascularization. Among capillary beds of the body, the brain is associated with the highest pericyte coverage (11). The endothelial basement membrane is secreted by endothelial cells and pericytes, the latter of which are embedded in this membrane. The parenchymal or astrocytic basement membrane is secreted by astrocytes (13). Astrocytes are glial cells with end-feet that cover the basolateral surface of endothelial cells. Cross-talk between astrocytes and endothelial cells regulates many barrier functions of the endothelia (14).

The neurovascular unit includes the BBB, neurons, microglial cells, and potentially infiltrating immune cells (15). Microglia are resident immunocompetent cells of the brain. Both microglia and astrocytes are subject to activation in neuroinflammatory responses, seen in both experimental mouse brain metastases and human craniotomy specimens (16, 17). In the neuroinflammatory response, astrocytes loosely surround, rather than directly bind vessels.

Herein, we describe a new model of experimental brain metastasis of HER2$^+$ breast cancer, the SUM190-BR3 line. Brain metastasis permeability is quantified in three model systems. Using these tools, we characterize the nature of the BTB and neuroinflammatory process. Our data identify numerous differences between uninvolved brain (no metastases) and brain metastases. Alterations in two distinct subpopulations of pericytes (desmin$^+$ and CD13$^+$), and laminin α2 in the astrocytic basement membrane, were found to occur with greater metastasis permeability.

Materials and Methods

Animal experiments

All animal experiments were performed under approved NCI or West Virginia University Animal Use agreements. Derivation of the SUM190-BR3 subline is described in Supplementary Methods. To characterize the BBB in experimental brain metastases, three brain-tropic experimental models were investigated, 231-BR6 (18) derived from triple-negative MDA-MB-231 cells, JIMT-1-BR3 (19) derived from HER2$^+$ JIMT-1 cells (20), and SUM190-BR3 cells, derived from HER2$^+$ SUM190 inflammatory breast cancer cells (Supplementary Methods). The three brain-tropic cell lines have not been authenticated. All cell lines expressed GFP. The experimental metastasis assays, Texas Red dextran injections, and perfusion techniques are described in Supplementary Methods.

Experimental brain metastasis permeability

Quantification of Texas Red dextran uptake was performed as reported previously (7) and plotted using uninvolved brain as a reference. For immunofluorescence analysis of BBB and BTB components, 200 8-μm serial brain sections were cut in the sagittal plane (two sections per slide); every tenth slide was stained with H&E, and every fifth slide was analyzed microscopically by fluorescence for Texas Red dextran and eGFP to identify poorly permeable and highly impermeable parenchymal (but not olfactory) metastases. The slides in between the serial measurements of Texas Red dextran permeability were used for quantitative immunofluorescence (Supplementary Methods, Supplementary Tables S1 and S2 for the list of markers investigated by immunofluorescence).

Immunofluorescence of human craniotomy specimens

Anonymized snap-frozen human craniotomy specimens were obtained by IRB approval from Massachusetts General Hospital (Boston, MA) and the Military Institute of Medicine (Warsaw, Poland). Tissues were embedded in OCT, stained, and photographed as described in Supplementary Methods.

Image analysis

Images from all distinctly highly permeable and poorly permeable metastases in a section, and brain devoid of metastases (uninvolved brain), were acquired with the Zeiss Axioskop. Axiovision4 software was used to calculate percent area

stained by each immunofluorescence marker (Supplementary Methods).

Statistical analysis

Ratios (brain metastases to uninvolved brain or of highly permeable to poorly permeable metastases) were tested against a hypothetical value of one using the Wilcoxon signed-rank test (Supplementary Methods, Supplementary Table S3 for the summary of the statistical analysis of brain metastases vs. uninvolved brain and Supplementary Table S4 for the summary of the statistical analysis of highly permeable vs. poorly permeable brain metastases).

Results

SUM190-BR3 model system

To provide an additional experimental brain metastasis model that was HER2$^+$, the SUM190 human inflammatory breast cancer cell line was subjected to three rounds of intracardiac injection, sterile harvest of brain metastases 8 to 10 weeks later, and *ex vivo* culture, generating SUM190-BR3. HER2 staining was confirmed by immunofluorescence and was homogeneous (Supplementary Fig. S1).

Texas Red dextran permeability of three experimental brain metastasis model systems

The hypotheses to be tested are that experimental brain metastases of breast cancer exhibit consistent changes in their BTB and/or neuroinflammatory response (i) as metastases develop (in comparison with the BBB of the uninvolved brain) and (ii) as metastases change from lower permeability to higher permeability. Figure 1A presents representative hematoxylin and eosin (H&E)–stained images of lesions produced by triple-negative 231-BR6 cells, HER2$^+$ JIMT-1-BR3 cells, and HER2$^+$ SUM190-BR3 cells. The morphologies of the 231-BR6 and JIMT-1-BR3 lesions were similar, infiltrating small clusters

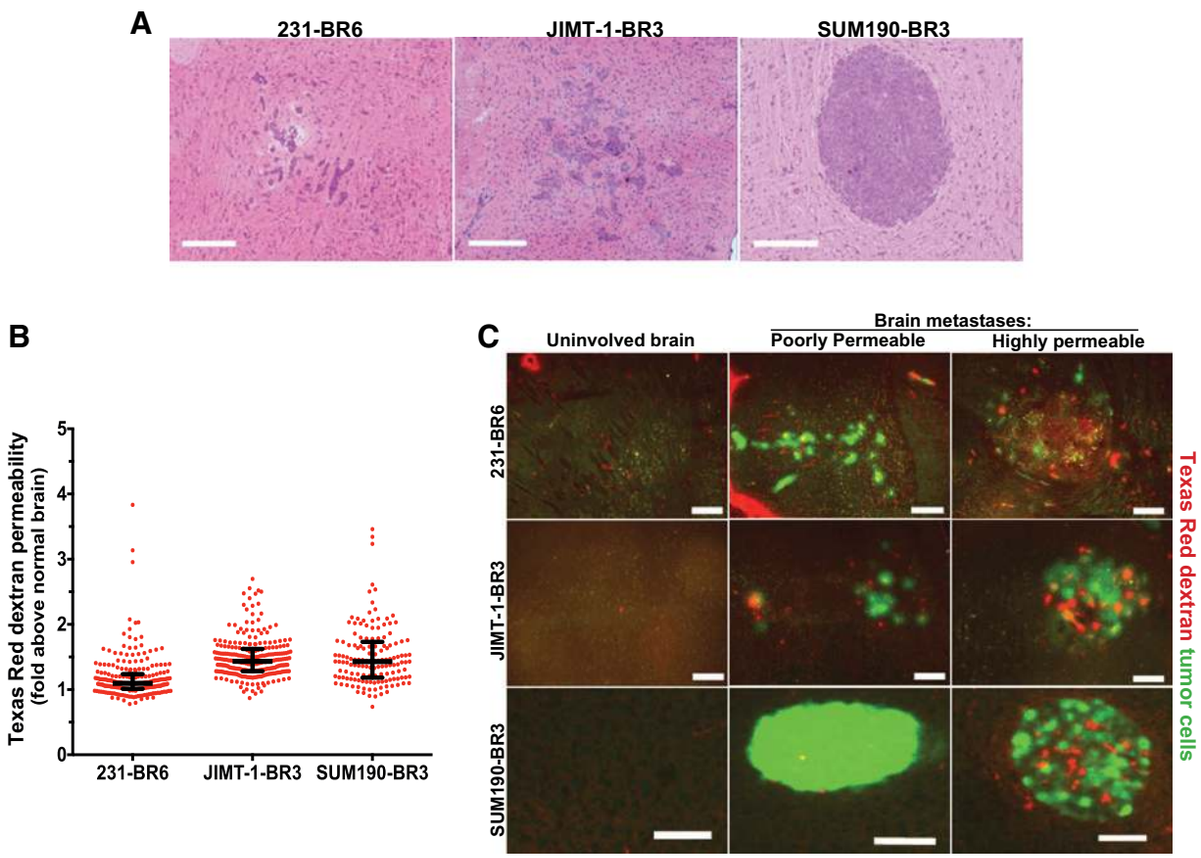

Figure 1.

Heterogeneous permeability of three experimental brain metastasis model systems of breast cancer to 3 kDa Texas Red dextran. Tumor cells from three human brain-tropic cell lines were each injected into the left cardiac ventricle of immunocompromised mice; just before necropsy mice were injected with 3 kDa Texas Red dextran. At necropsy, mice were perfused with saline such that the only Texas Red dextran remaining would be that permeable into tissue. **A**, Representative H&E-stained sections of the triple negative 231-BR6, HER2$^+$ JIMT-1-BR3, and inflammatory breast cancer SUM190-BR3 brain lesions. Scale bar, 300 μm. **B**, Texas Red dextran diffusion of 143–256 metastases/model system was determined by quantitative immunofluorescence (see Materials and Methods and Supplementary Methods) and plotted as a ratio of metastasis to the BBB in uninvolved brain (set at 1.0). Lines, median; bars, upper and lower quartiles. Each dot represents a single metastasis ($n = 5$ to 6 mice per group). **C**, For quantitative immunofluorescence analysis of BBB and neuroinflammatory response markers, highly and poorly permeable lesions within a single brain (tumor cells, green) were selected visually based on Texas Red diffusion. A representative photomicrograph of each is shown, along with uninvolved brain as a control. Scale bar, 200 μm (red, Texas red dextran; green, tumor cells). High permeability appeared as a diffuse cloud of red staining or areas of diffusion around vessels.

of tumor cells that may eventually coalesce, whereas SUM190-BR3 lesions were larger, roughly spherical, and occasionally centrally necrotic.

Texas Red dextran (3 kDa) was used as a permeability marker, as its exudation was well correlated with the permeability of AIB and drugs into experimental metastases (7, 8). Mice harboring experimental metastases were injected with Texas Red dextran and subsequently perfused to eliminate the dye from the vasculature just prior to necropsy. Figure 1B plots the range of Texas Red dextran permeability in 143–256 metastases per model system, compared with the permeability of uninvolved brain, which was uniformly negative and set at 1.0. The median permeabilities of the 231-BR6, JIMT-1-BR3, and SUM190-BR3 lesions were 1.1, 1.4, and 1.4-fold, respectively ($n = 5$ to 6 mice per group). Occasional lesions exhibited higher permeability, up to fourfold over uninvolved brain. Thus, although the histologies and sizes of the experimental brain metastases varied, their permeabilities exhibited similar ranges.

Within these ranges, the most permeable and impermeable metastases within a single mouse brain were selected visually (Fig. 1C). The pattern of Texas Red dextran exudation also varied by model system: high 231-BR6 metastasis permeability appeared as a cloud of red fluorescent staining as previously reported (7). High JIMT-1-BR3 metastasis permeability was evident around large intratumoral vessels. High SUM190-BR3 permeability was evident around large intratumoral vessels and/or peritumorally. The relative expression levels of BBB and neuroinflammatory components were then correlated with permeability.

Experimental schema for quantitative immunofluorescence of neuroinflammatory and BBB/BTB proteins

Brains from experimental metastasis assays were serially sectioned; every tenth slide was H&E stained to identify uninvolved brain and metastases, and every fifth slide examined for Texas Red dextran exudation to identify poorly and highly permeable metastases. The brain sections in between these benchmarks were used for quantitation. BBB and neuroinflammatory components were identified by immunofluorescence staining. The expression level of each marker was quantified and normalized to microscopic field area (for uninvolved brain), metastasis area (for markers in the microenvironment), or endothelial CD31 area (for proteins surrounding endothelial cells in the BBB). Two comparisons were made: the medians of all brain metastases versus uninvolved brain and within brain metastases, the medians of those that were distinctly highly permeable versus poorly permeable. Each distribution of ratios is shown as a box-and-whisker plot (whiskers extend to the minimum and maximum values) presenting the combined data for all quantified lesions within a single mouse brain as a dot.

The neuroinflammatory response

Sections of brains from the three model systems were stained for GFAP in activated astrocytes and CD11b/CD45 in activated microglia. Representative immunofluorescent images of activated astrocytes are shown in Fig. 2A. Virtually absent from the normal brain, overexpression of GFAP by astrocytes was a hallmark of the metastatic microenvironment, within and around lesions (Fig. 2A), as previously reported in human brain metastasis craniotomy specimens (16). When quantified as a percentage of lesion area and compared with uninvolved brain, GFAP staining increased 43.3-fold in the 231-BR6 model system ($P = 0.002$, $n = 10$), 41.3-fold in the JIMT-1-BR3 model system ($P = 0.002$, $n = 10$), and 10.02-fold in the SUM190-BR3 model system ($P = 0.008$, $n = 8$; Fig. 2B). Among the metastases, however, no difference was observed in the GFAP staining of highly permeable versus poorly permeable metastases (Fig. 2C; all $P > 0.25$).

Representative immunofluorescent images of activated microglia are shown in Fig. 2D. Activated microglia were increased over uninvolved brain 13.9-fold in the 231-BR6 model system ($P = 0.016$, $n = 7$), 619-fold in the JIMT-1-BR3 model system ($P = 0.002$, $n = 10$), and 15.1-fold in the SUM190-BR3 model system ($P = 0.016$, $n = 7$; Fig. 2E). No consistent differences were noted when poorly permeable and highly permeable metastases were compared (Fig. 2F). Activated microglia staining was 2.18-fold higher in highly permeable metastases in the 231-BR6 model (compared with poorly permeable metastases, $P = 0.016$, $n = 7$) but no statistically significant trend was observed in the JIMT-1-BR3 and SUM190-BR3 models [$P = 0.084$ ($n = 10$) and 0.47 ($n = 7$), respectively]. Other potential contributors to the neuroinflammatory response, such as infiltrating lymphocytes, were not assessed, as the experiments were performed in nude mice. Thus, alterations in the cellular expression of microglia and $GFAP^+$ astrocytes appear to be fundamental to the BTB but do not vary with higher versus lower lesion permeability.

BBB alterations in experimental brain metastases

A number of BBB components exhibited altered expression trends between uninvolved brain and brain metastases but did not vary between poorly and more highly permeable metastases (Fig. 3). $CD31^+$ endothelial capillaries were numerous and widely distributed throughout the uninvolved brain, and became much larger but less dense in metastatic lesions, in agreement with previous reports (7). CD31 expression was increased in brain metastases by 1.94-fold in 231-BR6 ($P = 0.0005$, $n = 12$), 2.04-fold in JIMT-1-BR3 ($P = 0.002$, $n = 10$), and 1.39-fold in SUM190-BR3 ($P =$ not significant, $n = 8$) models (Fig. 3B). When highly permeable to poorly permeable metastases were compared, expression ratios varied from 1.04 to 1.14 among the three models and were statistically insignificant (Fig. 3C, all $P > 0.10$). Claudin-5, an endothelial cell tight junction protein, demonstrated inconsistent trends when brain metastases were compared with uninvolved brain, and no trend was observed when poorly permeable and highly permeable metastases were compared (Supplementary Fig. S2).

VEGF is a proliferative factor for endothelia and has been implicated in brain metastasis formation in model systems (21–24) and in imaging (25). VEGF was overexpressed in brain metastases as compared with the uninvolved brain, 1.08×10^5-fold in the 231-BR6 ($P = 0.002$, $n = 10$), 358-fold in JIMT-1-BR3 ($P = 0.002$, $n = 10$), and 47.2-fold in SUM190-BR3 ($P = 0.016$, $n = 7$; Fig. 3D, top, and Supplementary Fig. S3). VEGF staining was 4.61-fold higher in highly permeable metastases in the JIMT-1-BR model (compared with poorly permeable metastases $P = 0.010$, $n = 10$), but no statistically significant trend was observed in the 231-BR6 or SUM190-BR3 models (Fig. 3D, bottom, both $P > 0.60$).

Both the tight junction adaptor protein (ZO-1) in endothelia and the aquaporin (AQP4) water channel in astrocyte end-feet were decreased in the BTB as compared with uninvolved brain (Fig. 3E and F, top, respectively, and Supplementary Figs. S4 and S5). In metastases, AQP4 was not uniformly localized to the

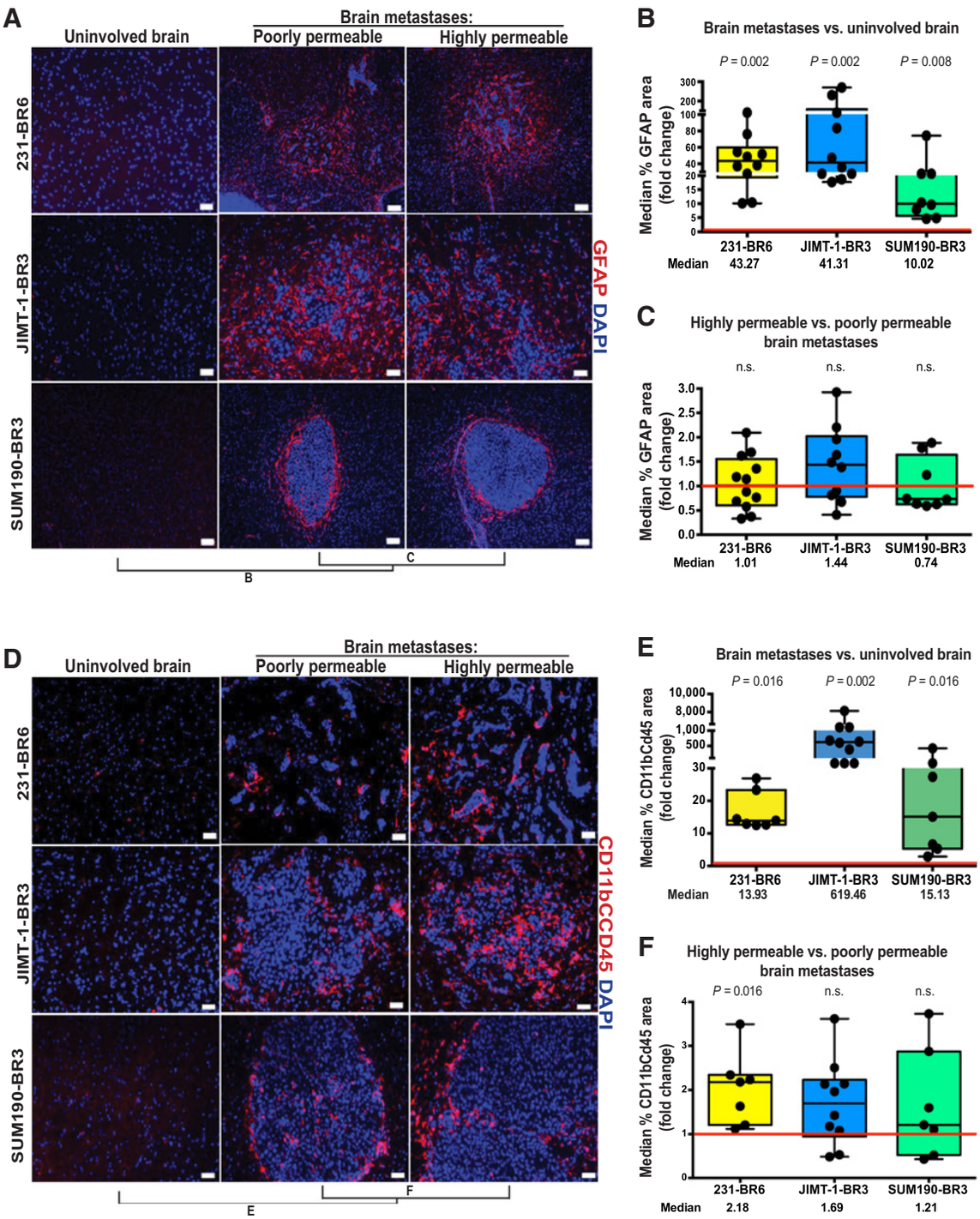

Figure 2.

Activated astrocytes and microglia in the neuroinflammatory response are quantitatively increased in experimental brain metastases. For the three model systems described in Fig. 1, metastases with distinctly high and low permeability to Texas Red dextran were identified within each animal brain, and adjoining tissue sections were stained for GFAP in activated astrocytes (**A**–**C**) or CD11b/CD45 in activated microglia (**D**–**F**). Staining was quantified using Axiovision4 software, normalizing to the area of the metastasis. For uninvolved brain, staining was quantified in the entire microscopic field. **A** and **D**, GFAP (**A**) Staining is shown as red in all three model systems and counterstained with DAPI (blue). Scale bar, 50 μm (231-BR6 and JIMT-1-BR3) and 100 μm (SUM190-BR3). CD11b/CD45 (**D**) Staining is red for all model systems. Scale bar, 50 μm. **B** and **E**, Expression of GFAP (**B**) and CD11b/CD45 (**E**) In all metastatic lesions in an animal was compared with that of uninvolved brain, with the compiled data from each animal shown as a dot. 1.0 (red line) indicates unity with uninvolved brain. *P* values are shown above each model and indicate that expression was increased in metastatic lesions (compared with uninvolved brain) in all three models. **C** and **F**, distinctly poorly and highly permeable metastases from a single mouse brain were compared, as described above, for GFAP (**C**) and CD11b/CD45 (**F**). n.s., not significant. All distributions overlapped the 1.0 unity line and did not demonstrate a statistical trend, with the exception of 231-BR6 cells for activated microglial staining.

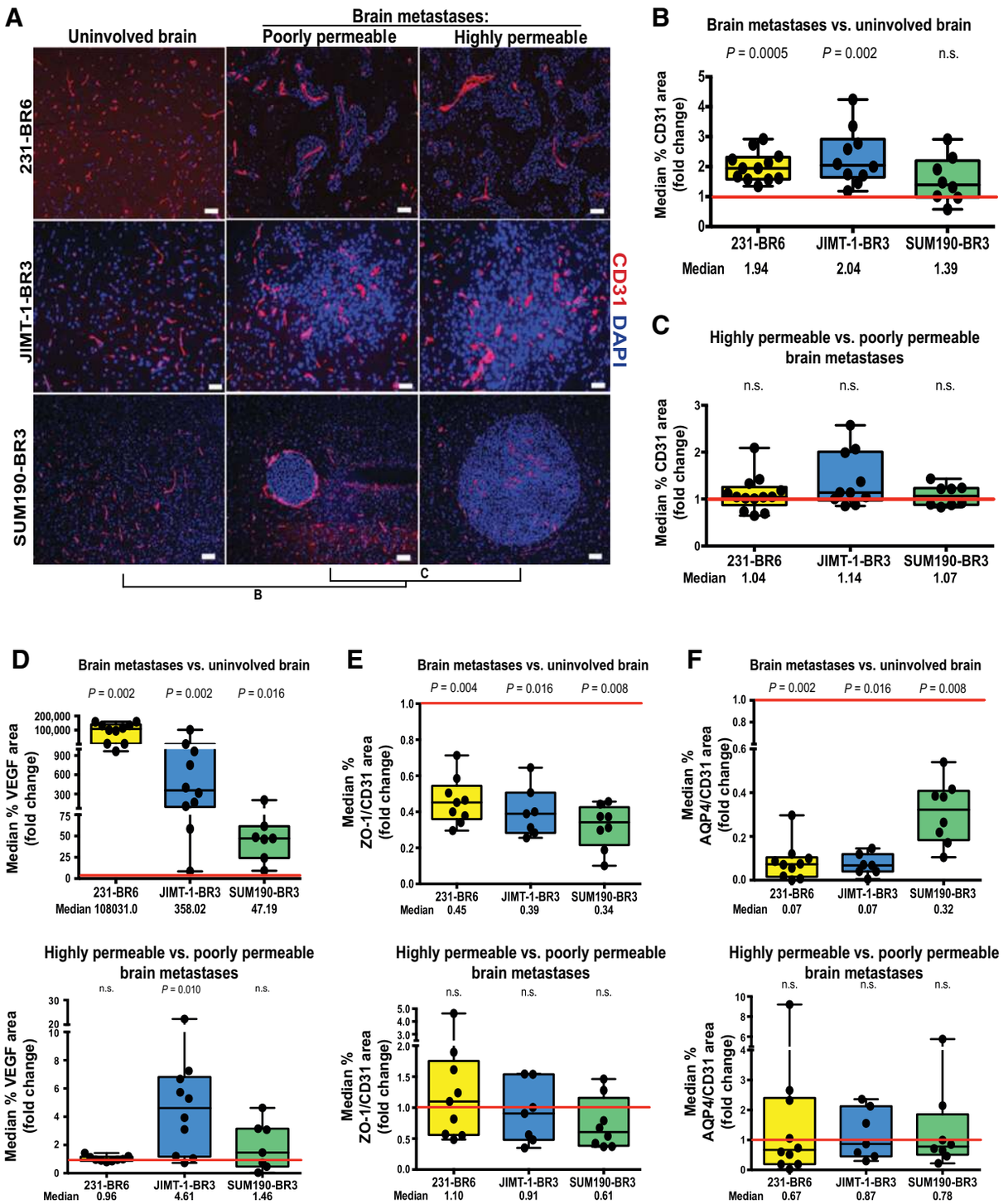

Figure 3.

Widespread alterations in the BTB. For the model systems described in Fig. 1, quantitative immunofluorescence was conducted for the CD31 area of endothelial cells (**A** and **B**), VEGF (**D**, top), zona occludens-1 tight junction protein (ZO-1, **E**, top), and the aquaporin 4 water channel in astrocyte end-feet (AQP4, **F**, top; see Materials and Methods and Supplementary Methods). Data were plotted as described in Fig. 2, with each dot representing the combined lesions of a single mouse brain and the red line indicating unity. Median fold change is listed below, and *P* values are listed above the plots. All markers demonstrated a statistically significant alteration in expression, when compared with uninvolved brain, in at least two of the model systems. A similar comparison of more permeable to less permeable metastases is shown in **A** and **C**, and the bottom of **D**–**F**. n.s., not significant. Staining was quantified as described in Fig. 2, except that metastasis images were normalized to CD31 staining for **B**–**D**. Scale bar (**A**), 50 μm (231-BR6 and JIMT-1-BR3) and 100 μm (SUM190-BR6). None of these markers was consistently correlated with low versus high BTB permeability.

astrocytic end-feet immediately surrounding the blood vessels, but occurred more distally, suggesting a loss of polarization of astrocyte end-feet (Supplementary Fig. S5B). No significant differences were observed when highly permeable and poorly permeable metastases were compared (Fig. 3E and F, bottom, all $P > 0.05$). Type IV collagen is a constituent of the endothelial and astrocytic basement membranes in the BBB. Representative photomicrographs and quantification of staining demonstrate heterogeneous trends of collagen IV/CD31 ratio in uninvolved brain versus brain metastases, with an increase in the 231-BR6 ($P = 0.02$, $n = 10$), whereas the other models tended to show a decrease but remained nonsignificant (Supplementary Fig. S6). No trend was observed between highly permeable and poorly permeable brain metastases in all three models. In summary, the BTB involves consistent changes in multiple cell components of the BBB, which do not appear to be further altered between poorly and more highly permeable metastases.

Decreases in the parenchymal basement membrane component laminin α2 correlates with an increase in BTB permeability

Staining for laminin α2, a component of the astrocytic basement membrane, is shown in Fig. 4A. Diffuse staining along vessels was apparent in uninvolved brain. When laminin α2/CD31 staining was quantified, it was consistently decreased in the BTB as compared with uninvolved brain: 58% in 231-BR6 metastases ($P = 0.001$, $n = 11$), 47% in JIMT-1-BR3 metastases ($P = 0.002$, $n = 10$), and 68% in SUM190-BR3 metastases ($P = 0.008$, $n = 8$; Fig. 4B). When highly permeable metastases were compared with poorly permeable metastases in the same brain, a further reduction in laminin α2 staining was observed. Laminin α2 staining in highly permeable lesions was reduced by 26% in 231-BR6 lesions ($P = 0.001$, $n = 12$), by 21% in JIMT-1-BR3 lesions ($P = 0.049$, $n = 10$), and by 40% in SUM190-BR3 ($P = 0.023$, $n = 8$) lesions compared with visually less permeable lesions (Fig. 4C). These data stand in contrast to the basement membrane component type IV collagen as described previously.

Altered metastasis permeability is associated with pericyte subpopulations

Platelet-derived growth factor (PDGF) receptor-β (PDGFR-β) is the best described marker for pericytes, and PDGFR knockout or hypomorphic mice exhibit BBB leakiness (26, 27). PDGFR-β staining normalized to CD31 in the three model systems is shown in Fig. 5A–C. PDGFR-β^+ pericytes decreased in expression in the BTB as compared with uninvolved brain by 75% in the 231-BR6 ($P = 0.016$, $n = 7$) and 69% in the JIMT-1-BR3 ($P = 0.016$, $n = 7$) models, while no significant changes were observed in the SUM190-BR3 model (Fig. 5B). No trends in expression were observed between highly and poorly permeable metastases in all the three models (Fig. 5C, all $P > 0.45$).

To more precisely capture the dynamic role of pericyte subpopulations in the context of brain metastases, we stained for two reported subpopulation markers, desmin and CD13. Desmin is a type III intermediate filament structural protein that identifies a subpopulation of pericytes in the CNS, skeletal muscle, and heart (15). Figure 5D–F quantifies desmin expression normalized to CD31. Desmin$^+$ pericytes faintly surrounded the vessels of the

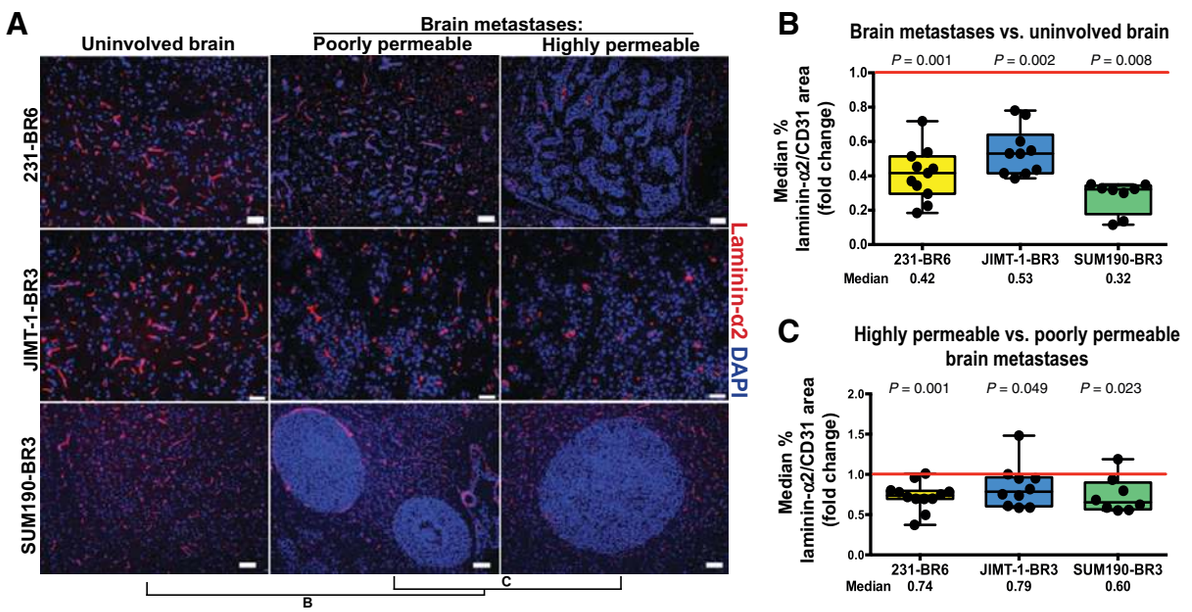

Figure 4.

Loss of laminin α2 in the astrocytic basement membrane is indicative of both the BTB and of higher metastasis permeability. **A**, Laminin α2 staining of brain sections from the three model systems was conducted as described in the Fig. 2 legend; laminin α2 staining is shown as red against blue DAPI nuclei. CD31 staining for normalization in tumor specimens was conducted on the adjacent tissue section due to a requirement for the same secondary antibody. Scale bar, 50 μm (231-BR6 and JIMT-1-BR3) and 100 μm (SUM190-BR3). **B**, Quantification of laminin α2/CD31 ratio in brain metastases compared with uninvolved brain, conducted as described in Fig. 2, showed a statistically significant reduction in expression in the BTB of all model systems. **C**, Comparison of laminin α2/CD31 ratio in distinctly poorly and highly permeable metastases within the same mouse brain, as described in Fig. 2, showed a reduction in laminin α2 expression in the most permeable metastases of all three model systems, statistically significant in the 231-BR6 model and strong trends in the others.

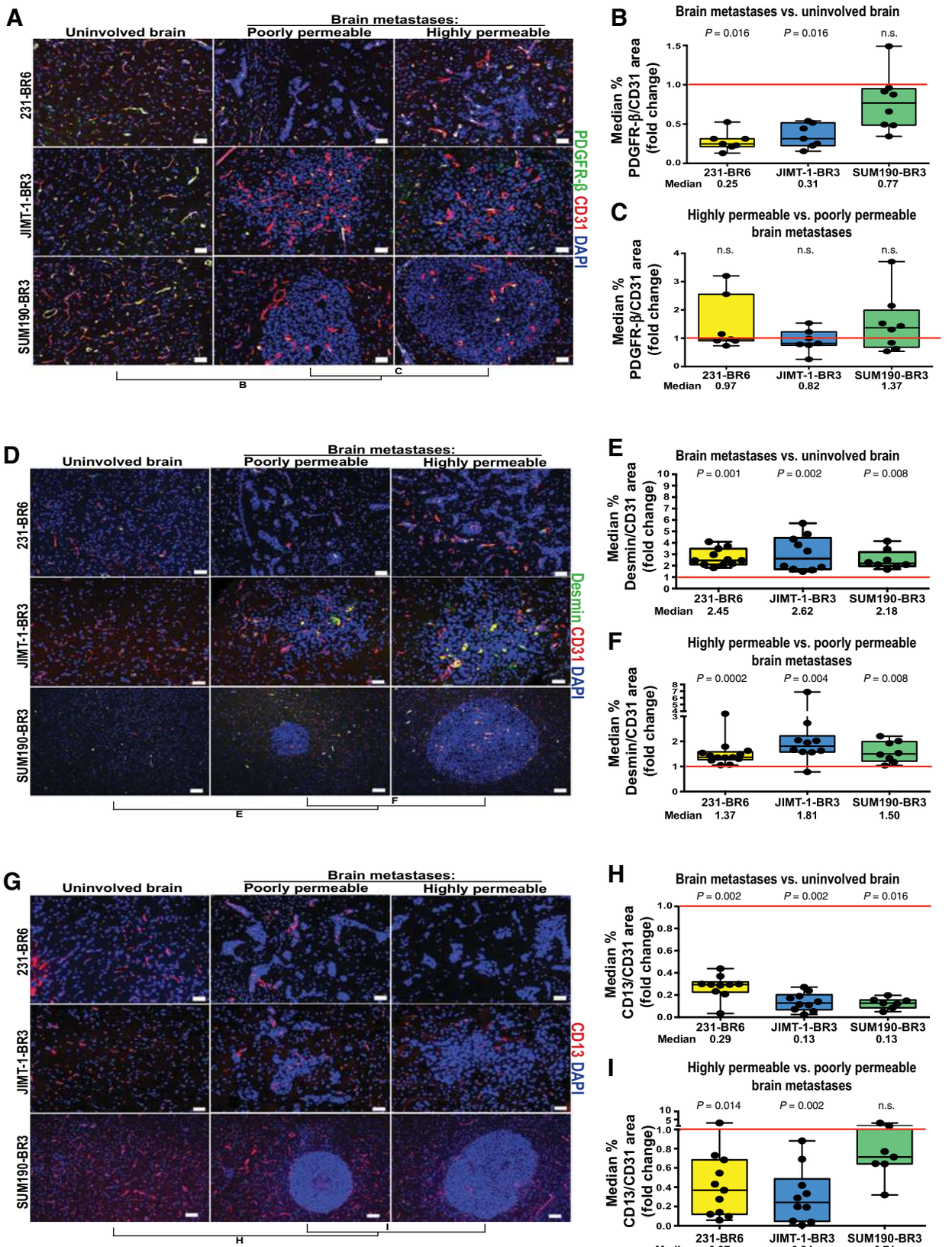

uninvolved brain. For all three models, desmin/CD31 was increased in brain metastases as compared with uninvolved brain, 2.45-fold in the 231-BR6 model ($P = 0.001$, $n = 11$), 2.62-fold in the JIMT-1-BR3 model ($P = 0.002$, $n = 10$), and 2.18-fold in the SUM190-BR3 model ($P = 0.008$, $n = 8$). When metastases poorly and highly permeable to Texas Red dextran were compared, highly permeable lesions exhibited a greater amount of desmin/CD31, 1.37-fold in the 231-BR6 model ($P = 0.0002$, $n = 13$), 1.81-fold in the JIMT-1-BR3 model ($P = 0.004$, $n = 10$), and 1.50-fold in the SUM190-BR3 model ($P = 0.008$, $n = 8$). Using confocal microscopy, costaining for desmin and PDGFR-β in JIMT-1-BR3 brain metastases showed a median overlap of 74.1%, with a wide range, from 14.5% to 98.5% among individual lesions (Supplementary Fig. S7).

CD13 encodes alanyl membrane aminopeptidase, which stains a subpopulation of pericytes as well as vascular smooth muscle cells, myeloid cells, and kidney/gut epithelial cells (15). Figure 5G–I quantifies CD13 expression as a percentage of $CD31^+$ vessel area. For all three models, CD13/CD31 was decreased in brain metastases as compared with uninvolved brain, 71% in the 231-BR6 model ($P = 0.002$, $n = 10$), 87% in the JIMT-1-BR3 model ($P = 0.002$, $n = 10$), and 87% in the SUM190-BR3 model ($P = 0.016$, $n = 7$). When metastases poorly and highly permeable to Texas Red dextran were compared, permeable lesions exhibited a lower amount of CD13/CD31 in two model systems, 63% in the 231-BR6 model ($P = 0.014$, $n = 11$) and 76% in the JIMT-1-BR3 model ($P = 0.002$, $n = 10$). For SUM190-BR3 metastases, a moderate 29% decrease was observed but was not significant ($P = 0.29$, $n = 7$). Vessels from JIMT-1-BR3 brain metastasis were costained for CD13 and PDGFR-β and analyzed by confocal microscopy to determine the extent in overlap in expression. The median overlap of CD13 and PDGFR-β staining in JIMT-1-BR3 metastases was 56.8%, with a wide range, from 21.5% to 84.5% among individual lesions (Supplementary Fig. S7). In summary, although PDGFR-β identified a broad pericyte population, including both $desmin^+$ pericyte and $CD13^+$ pericyte populations, desmin and CD13 markers unmasked two distinct pericyte populations, with only 12% colocalization and with opposite patterns of expression related to metastasis permeability.

Human craniotomy specimens

We asked whether $desmin^+$ pericytes, the subpopulation associated with increased permeability in mouse models, occur in human brain metastases. As immunofluorescence with this antibody required snap-frozen tissue, relatively few craniotomy specimens from patients with breast and lung cancer were available. Nine of 14 specimens collected were well preserved, and seven among 13 antibodies tried gave a specific staining (Supplementary Table S5 for the list of antibodies that could not be quantified and Supplementary Table S6 for the analysis of human brain metastasis specimens with specific antibodies). Among the nine specimens, one was devoid of tumor cells (specimen #6, Supplementary Table S6). Comparing this specimen with other specimens with high tumor cell contents, a comparison of $CD13^+$ and $desmin^+$ pericytes in uninvolved brain versus metastatic lesions was feasible (Fig. 6A). Vessels, identified by collagen IV staining, were covered primarily by $CD13^+$ pericytes in the uninvolved brain. In brain metastases, $desmin^+$ pericytes covered the vessels. $Desmin^+$ pericytes covered the vessels in characteristic patterns in seven of nine craniotomy specimens (Supplementary Table S6; Supplementary Fig. S8). Additional components of the BTB and neuroinflammatory response that were identified are shown in Supplementary Fig. S9 and tabulated on Supplementary Table S6.

Discussion

Of the model systems used, the triple-negative 231-BR6 model has been widely reported (18) and a $HER2^+$ JIMT-1-BR3 model was recently developed (19). A new SUM190-BR3 model provides an independent $HER2^+$ brain metastasis model and is from inflammatory breast cancer (IBC). IBC constitutes approximately 1% to 6% of breast cancer cases. Brain metastasis is estimated to affect 16% of patients with IBC within 20 months of a metastatic diagnosis and was associated with a median survival of 6 months (28). A proportion of SUM190-BR3 brain metastases have central necrosis, a feature of some human brain metastases not yet seen in the models developed to date.

The debate on the "openness" of the BTB, once a brain metastasis has formed, continues. Despite the facts that brain metastases image with gadolinium and turn variably blue in mice injected with dye (5), most of the data indicate that the BTB is not open "enough" for therapy to be effective. Many chemo- and molecular therapy trials for brain metastases have been uniformly disappointing even when the agents had systemic activity in the extracranial metastatic setting (e.g., refs. 29–32). Using two triple-negative experimental brain metastasis model systems, uptake of two markers (AIB and Texas Red dextran) or radiolabeled paclitaxel was heterogeneous, with approximately 87% of metastases more permeable than normal brain, but only 10% of lesions showing high enough paclitaxel permeability to elicit a cytotoxic response. Similar heterogeneous uptake of doxorubicin and lapatinib was also reported (7, 8). Texas Red dextran

Figure 5.

Desmin$^+$ pericytes identify highly permeable brain metastases. For the three model systems described in Fig. 1, metastases with distinctly high and low permeability to Texas Red dextran were identified within each animal brain, and adjoining tissue sections were stained for three markers of pericytes: PDGFR-β (**A–C**), desmin (**D–F**), and CD13 (**G–I**). Quantitative immunofluorescence of each marker in uninvolved brain versus metastasis and poorly versus highly permeable metastases was plotted as described in Fig. 2. **A–C**, PDGFR-β^+ pericytes (green) normalized to CD31 (**A**). PDGFR-β^+ pericyte coverage was decreased in metastases as compared with uninvolved brain in the 231-BR6 and JIMT-1-BR3 model systems (**B**) but was unrelated to metastasis permeability in all three models (**C**). n.s., not significant. Scale bar, 50 μm. **D–F**, expression of the desmin$^+$ subpopulation of pericytes (green) normalized to CD31 (**D**) by the same methods (yellow, costain). The data show both a significant increase in desmin$^+$ pericyte expression when brain metastases were compared with uninvolved brain (**E**) as well as increased expression in more permeable metastases as compared with less permeable metastases in the same brain (**F**). Scale bar, 50 μm (231-BR6 and JIMT-1-BR3) and 100 μm (SUM190-BR3). **G–I**, Expression of the CD13$^+$ subpopulation of pericytes (**G**) normalized to CD31 (in an adjacent section) by the same methods. The data demonstrate both a decrease in CD13$^+$ pericyte expression when brain metastases were compared with uninvolved brain (**H**), as well as a strong trend of further decreased expression in more permeable metastases as compared with less permeable metastases in the same brain in the 231-BR6 and JIMT-1-BR3 models (**I**). Scale bar, 50 μm (231-BR6 and JIMT-1-BR3) and 100 μm (SUM190-BR3).

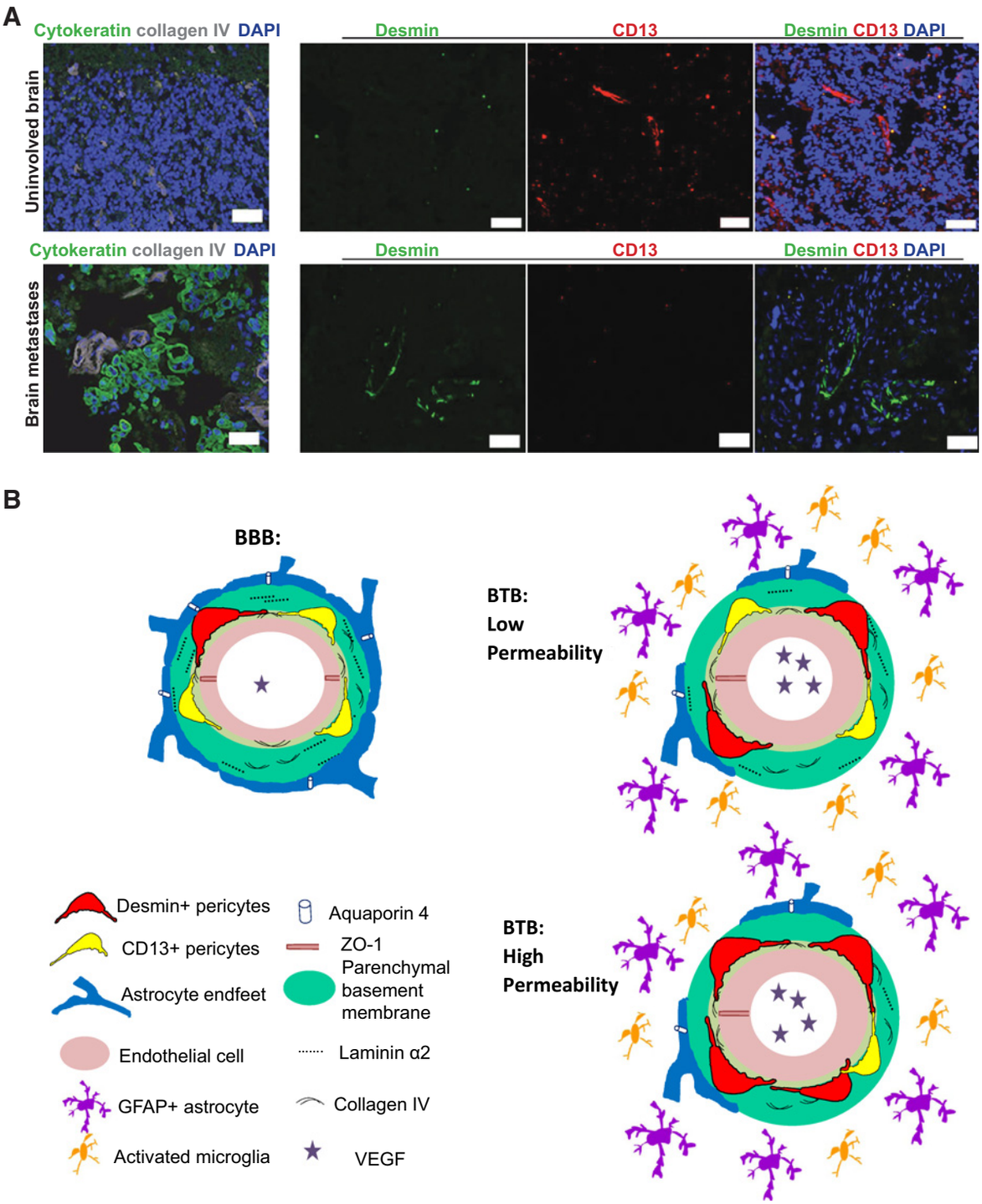

Figure 6.
Identification of pericyte desmin expression in human craniotomy specimens and data summary in a graphic model. **A**, In uninvolved brain [i.e., devoid of human cytokeratin-positive tumor cells (green; top row)] from a human craniotomy specimen, small caliber vessels are identified by collagen IV staining (gray). $CD13^+$ (red) pericytes are observed while $desmin^+$ pericytes (green) are virtually absent. In a human specimen with a high tumor cell content (identified with cytokeratin in green; bottom row), dilated blood vessels are identified by collagen IV (gray). There is increased expression of $desmin^+$ pericytes (green), and $CD13^+$ pericytes (red) are absent. **B**, Model of the BBB and BTB in experimental brain metastases of breast cancer. Left, the BBB components studied are shown. Endothelial cell (pink) with ZO-1 tight junction adaptor protein and VEGF within the lumen. Adjacent endothelial basement membrane (light green) and adjoining astrocytic basement membrane (teal), both containing type IV collagen (arc lines); laminin α2 as dotted line in the astrocytic basement membrane. Astrocyte end-feet (blue) with aquaporin 4 (AQP4) water channels, white. Right, the BTB under conditions of relatively low (top) and high (bottom) permeability to Texas Red dextran. Consistent changes in the formation of a BTB include dilation of endothelial cells, increased $desmin^+$ pericytes, abundant VEGF, and decreases in ZO-1, laminin α2, AQP4, and $CD13^+$ pericytes. A prominent neuroinflammatory response of activated astrocytes (purple) and microglia (orange) surrounds the BTB. Higher BTB permeability is associated with further increased $desmin^+$ pericytes, decreased $CD13^+$ pericytes, and laminin α2 in the parenchymal basement membrane.

permeability was directly correlated with peptide, paclitaxel, and doxorubicin permeability in the mouse models (all $P < 0.0001$; ref. 7), validating its use herein as a general marker. The leakiness of experimental brain metastases in the three model systems confirms and extends these trends, showing median fold changes over uninvolved brain from 1.1- to 1.4-fold, with occasional more permeable metastases up to fourfold.

Our central hypothesis is that an understanding of the cellular and molecular changes inherent in the transformation of the BBB to a BTB, and then from a poorly permeable to a more highly permeable BTB, may identify targetable pathways to improve drug therapy. Prior studies in this field reported that 11- to 13-nm "pores" open in the BTB (33), that TNF–TNFR1 pathway induces BTB permeabilization (34) and that angiopoietin-2 destabilized endothelial tight junctions (35). The BBB is often studied in models of brain injury or neurodegenerative disorders, such as stroke, multiple sclerosis, or Alzheimer disease, where the overall goal is to reinstate BBB function. Fluorescent microscopy is the primary tool used to ascertain which proteins are present and bound to what structure, with blood protein or dye penetration as a readout of permeability. Taking this cue, we quantitated the expression of multiple BBB markers in the most and least Texas Red dextran–positive lesions within a single brain.

The data indicate that the formation of a BTB from a BBB is not a random breakdown of the BBB, but a series of consistent alterations, with some facets increasing in expression while others are diminished (Fig. 6B). Briefly, the formation of a BTB involves dilation of vessels (increased CD31 area), increased levels of VEGF, and a prominent neuroinflammatory response (increased GFAP-overexpressing astrocytes and CD11b/CD45–activated microglia). Decreased expression of the endothelial ZO-1 tight junction adaptor protein and the AQP4 water channel in astrocyte end-feet was observed. Each of the changes noted in the BTB may also contribute to limited BTB permeability, lower than the permeability levels associated with paclitaxel cytotoxicity (7).

The most interesting difference observed in BBB expression patterns may be those that are correlated with low versus high permeability (Fig. 6B). High permeability of the BTB to Texas Red dextran was associated with an increase in desmin$^+$ pericyte coverage of the endothelia, a heterogeneous decrease in CD13$^+$ pericyte coverage, and reduced expression of laminin α2 in the parenchymal basement membrane. Pericytes are mural cells found throughout the body. They contribute to glioblastoma progression and metastasis in systemic models (36–38). The brain has the highest pericyte coverage (11). Abnormal pericyte coverage and function has been implicated in CNS diseases, including diabetic retinopathy, stroke, and neurodegeneration (39). In the brain, pericytes regulate the expression of tight and adherens junction components, transcytosis, extracellular matrix production, and vascular stability to maintain BBB integrity (27, 39). Endothelial cell–derived PDGF-β, secreted into the basement membrane, attracts pericytes via their PDGFR-β receptors, and PDGFR-β–null or hypomorphic mice were pericyte deficient with an impaired BBB (26, 27). Pericytes being a plastic and heterogeneous population, different markers are required to identify them. The most frequently used markers are PDGFR-β, NG2 chondroitin sulfate proteoglycan, CD13 alanyl membrane aminopeptidase, the structural protein desmin, and α smooth muscle actin (αSMA), each of them being variably expressed depending on developmental stage, organs investigated or pathologic conditions (reviewed in ref. 15). Of these, we were unable to validate antibodies to NG2 using Texas Red dextran permeability fixation conditions; αSMA was undetectable in uninvolved brain and metastases using the Sigma (A2547) antibody in our model systems. Pericyte PDGFR-β expression decreased in brain metastases as compared with uninvolved brain in the three models, but there was only a statistical trend in the 231-BR6 and JIMT-1-BR3 models. No trend was observed comparing high permeability versus low metastasis permeability.

Interestingly, two distinct pericyte subpopulations were identified with opposite correlations with BTB permeability. CD13$^+$ pericyte coverage of endothelial cells decreased in the most permeable lesions in two models, 63% in 231-BR6 and 76% in JIMT-1-BR3. In the SUM190-BR3 model system, no significant change was noted. The magnitude of the decreases in the 231-BR6 and JIMT-1-BR3 model systems suggests that this alteration may have potent, although not universal functionality. Conversely, desmin$^+$ pericyte coverage of endothelial cells increased in brain metastases as compared with uninvolved brain and was further increased in highly permeable metastases by 1.4-fold in the 231-BR6 model, 1.8-fold in the JIMT-1-BR3 model, and 1.5-fold in the SUM190-BR3 model as compared with less permeable lesions. To our knowledge, this is the first demonstration of altered pericyte subpopulations in metastatic BTB permeability.

Desmin-positive and negative pericyte subpopulations have been reported in a mouse model of spinal cord injury (40). The desmin$^-$ subpopulations exhibited a proliferative and migratory phenotype in contrast to desmin$^+$ pericytes. As the desmin$^-$ pericytes migrated away from the blood vessels, they lost CD13 expression (40). These data illustrate the dynamic phenotype of pericytes in another pathologic context. Taken together, the data suggest the hypotheses that pericyte subpopulations are regulated in distinct manners, potentially have distinct functions, and that their altered prevalence can functionally alter BTB permeability. It is tempting to speculate that CD13$^+$ pericytes transform into desmin$^+$ pericytes, although other origins for the increased desmin$^+$ pericytes include their own expansion, a bone marrow source, and potentially endothelial origin through endothelial–mesenchymal transitions (41). Finally, using immunofluorescence, we identified desmin$^+$ pericytes covering vessels in seven of nine human craniotomy specimens analyzed.

Another interesting finding is that laminin α2, found in the parenchymal basement membrane of the BBB, was reduced in the highly permeable BTB of the three model systems by 21% to 40% as compared with poorly permeable metastases. Using conditional gene knockdown in a mouse model and functional *in vitro* experiments, astrocytic laminin was demonstrated to prevent pericyte differentiation to a contractile stage, thus maintaining BBB function (42). These data suggest the additional hypothesis that astrocytic production of laminin α2 controls pericyte differentiation and function in the context of the BTB.

Our work has limitations. Expression was quantified by immunofluorescence, and the signal depends on antibody specificity and sensitivity. It remains possible that smaller differences in antigen expression were not detected and that other cell types expressing low levels of antigens could contribute to the trends observed. Other cell types and markers may also play functional roles in BTB permeability; our work was limited by the number of antibodies compatible with the fixation

requirements for Texas Red dextran visualization (Supplementary Table S2). Notable among this list are the efflux pumps, or ABC transporters, which play an important role in the BBB function as they pump out xenobiotics. Two are well described for their drug resistance property: ABCB1 or P-glycoprotein and ABCG2 or breast cancer resistance protein. We previously reported no difference in ABCB1 expression in the 231-BR model between poorly and highly permeable metastases (7). We could not confirm this observation in the JIMT-1-BR3 model, as both tumor cells and endothelial cells expressed a high level of ABCB1. The ABCG2 antibody did not work under the fixation conditions used to determine permeability and could not be investigated. Permeability in our model systems was quantified by Texas Red dextran diffusion, thought to visualize paracellular extravasation. Although this marker has been extensively correlated with peptide and drug permeability, it remains possible that transcellular or other permeability mechanisms are distinctly regulated. Mechanistic experiments are required to prove a functional contribution of the alterations identified herein.

In summary, alterations in pericyte subpopulations and parenchymal basement membrane laminin α2 are associated with the transition of the BTB to higher states of permeability in three models of brain metastasis of breast cancer. These findings provide novel insights into the regulation of the BTB and potential translational approaches to improve chemotherapeutic uptake into brain metastases.

Disclosure of Potential Conflicts of Interest

P.K. Brastianos reports receiving speakers bureau honoraria from Genentech and Merck and is a consultant/advisory board member for Genentech. P.S. Steeg reports receiving a commercial research grant from Genentech. No potential conflicts of Interest were disclosed by the other authors.

Authors' Contributions

Conception and design: L.T. Lyle, P.S. Steeg, B. Gril
Development of methodology: L.T. Lyle, P.R. Lockman, D. Palmieri, B. Gril
Acquisition of data (provided animals, acquired and managed patients, provided facilities, etc.): L.T. Lyle, P.R. Lockman, C.E. Adkins, A.S. Mohammad, E. Hua, E. Izycka-Swieszewska, R. Duchnowska, P.K. Brastianos, B. Gril
Analysis and interpretation of data (e.g., statistical analysis, biostatistics, computational analysis): L.T. Lyle, P.R. Lockman, C.E. Adkins, A.S. Mohammad, E. Sechrest, D.J. Liewehr, S.M. Steinberg, P.S. Steeg, B. Gril
Writing, review, and/or revision of the manuscript: L.T. Lyle, P.R. Lockman, C.E. Adkins, A.S. Mohammad, D. Palmieri, D.J. Liewehr, S.M. Steinberg, W. Kloc, P.K. Brastianos, P.S. Steeg, B. Gril
Administrative, technical, or material support (i.e., reporting or organizing data, constructing databases): L.T. Lyle, E. Izycka-Swieszewska, N. Nayyar, B. Gril
Study supervision: L.T. Lyle, P.S. Steeg, B. Gril
Other (operational development of clinical material and preparation of the tumor for laboratory tests): W. Kloc

Grant Support

This work was supported by the Intramural Program of the NCI, U.S. Department of Defense Breast Cancer Research Program, grant number: W81 XWH-062-0033, and a research grant from the Inflammatory Breast Cancer Research Foundation.

The costs of publication of this article were defrayed in part by the payment of page charges. This article must therefore be hereby marked *advertisement* in accordance with 18 U.S.C. Section 1734 solely to indicate this fact.

Received August 3, 2015; revised April 25, 2016; accepted May 19, 2016; published OnlineFirst May 31, 2016.

References

1. Brufsky AM, Mayer M, Rugo HS, Kaufman PA, Tan-Chiu E, Tripathy D, et al. Central nervous system metastases in patients with HER2-positive metastatic breast cancer: incidence, treatment, and survival in patients from registHER. Clin Cancer Res 2011;17:4834–43.
2. Anders CK, Deal AM, Miller CR, Khorram C, Meng H, Burrows E, et al. The prognostic contribution of clinical breast cancer subtype, age, and race among patients with breast cancer brain metastases. Cancer 2011;117:1602–11.
3. Bendell J, Domchek S, Burstein H, Harris L, Younger J, Kuter I, et al. Central nervous system metastases in women who receive trastuzumab-based therapy for metastatic breast carcinoma. Cancer 2003;97:2972–7.
4. Lin NU, Amiri-Kordestani L, Palmieri D, Liewehr DJ, Steeg PS. CNS metastases in breast cancer: old challenge, new frontiers. Clin Cancer Res 2013;19:6404–18.
5. Do J, Foster D, Renier C, Vogel H, Rosenblum S, Doyle TC, et al. *Ex vivo* Evans blue assessment of the blood brain barrier in three breast cancer brain metastasis models. Breast Cancer Res Treat 2014;144:93–101.
6. Brastianos PK, Carter SL, Santagata S, Cahill DP, Taylor-Weiner A, Jones RT, et al. Genomic characterization of brain metastases reveals branched evolution and potential therapeutic targets. Cancer Discov 2015;5:1164–77.
7. Lockman PR, Mittapalli RK, Taskar KS, Rudraraju V, Gril B, Bohn KA, et al. Heterogeneous blood-tumor barrier permeability determines drug efficacy in experimental brain metastases of breast cancer. Clin Cancer Res 2010;16:5664–78.
8. Taskar KS, Rudraraju V, Mittapalli RK, Samala R, Thorsheim HR, Lockman J, et al. Lapatinib distribution in HER2 overexpressing experimental brain metastases of breast cancer. Pharm Res 2012;29:770–81.
9. Percy DB, Ribot EJ, Chen Y, McFadden C, Simedrea C, Steeg PS, et al. *In vivo* characterization of changing blood-tumor barrier permeability in a mouse model of breast cancer metastasis: a complementary magnetic resonance imaging approach. Invest Radiol 2011;46:718–25.
10. Morikawa A, Peereboom DM, Thorsheim HR, Samala R, Balyan R, Murphy CG, et al. Capecitabine and lapatinib uptake in surgically resected brain metastases from metastatic breast cancer patients: a prospective study. Neuro Oncol 2015;17:289–95.
11. Obermeier B, Daneman R, Ransohoff RM. Development, maintenance and disruption of the blood-brain barrier. Nat Med 2013;19:1584–96.
12. Bicker J, Alves G, Fortuna A, Falcao A. Blood-brain barrier models and their relevance for a successful development of CNS drug delivery systems: a review. Eur J Pharm Biopharm 2014;87:409–32.
13. Daneman R. The blood-brain barrier in health and disease. Ann Neurol 2012;72:648–72.
14. Abbott NJ, Ronnback L, Hansson E. Astrocyte-endothelial interactions at the blood-brain barrier. Nat Rev Neurosci 2006;7:41–53.
15. Armulik A, Genove G, Betsholtz C. Pericytes: developmental, physiological, and pathological perspectives, problems, and promises. Dev Cell 2011;21:193–215.
16. Fitzgerald DP, Palmieri D, Hua E, Hargrave E, Herring JM, Qian Y, et al. Reactive glia are recruited by highly proliferative brain metastases of breast cancer and promote tumor cell colonization. Clin Exp Metastasis 2008;25:799–810.
17. Lorger M, Felding-Habermann B. Capturing changes in the brain microenvironment during initial steps of breast cancer brain metastasis. Am J Pathol 2010;176:2958–71.
18. Palmieri D, Bronder JL, Herring JM, Yoneda T, Weil RJ, Stark AM, et al. Her-2 overexpression increases the metastatic outgrowth of breast cancer cells in the brain. Cancer Res 2007;67:4190–8.
19. Palmieri D, Duchnowska R, Woditschka S, Hua E, Qian YZ, Biernat W, et al. Profound prevention of experimental brain metastases of breast cancer by temozolomide in an MGMT-dependent manner. Clin Cancer Res 2014;20:2727–39.

20. Tanner M, Kapanen AI, Junttila T, Raheem O, Grenman S, Elo J, et al. Characterization of a novel cell line established from a patient with Herceptin-resistant breast cancer. Mol Cancer Ther 2004;3:1585–92.
21. Kienast Y, von Baumgarten L, Fuhrmann M, Klinkert WE, Goldbrunner R, Herms J, et al. Real-time imaging reveals the single steps of brain metastasis formation. Nat Med 2010;16:116–22.
22. Kim LS, Huang S, Lu W, Lev DC, Price JE. Vascular endothelial growth factor expression promotes the growth of breast cancer brain metastases in nude mice. Clin Exp Metastasis 2004;21:107–18.
23. Kusters B, Leenders WP, Wesseling P, Smits D, Verrijp K, Ruiter DJ, et al. Vascular endothelial growth factor-A(165) induces progression of melanoma brain metastases without induction of sprouting angiogenesis. Cancer Res 2002;62:341–5.
24. Eichler AF, Chung E, Kodack DP, Loeffler JS, Fukumura D, Jain RK. The biology of brain metastases-translation to new therapies. Nat Rev Clin Oncol 2011;8:344–56.
25. Leenders W, Kusters B, Pikkemaat J, Wesseling P, Ruiter D, Heerschap A, et al. Vascular endothelial growth factor-A determines detectability of experimental melanoma brain metastasis in GD-DTPA-enhanced MRI. Int J Cancer 2003;105:437–43.
26. Armulik A, Genove G, Mae M, Nisancioglu MH, Wallgard E, Niaudet C, et al. Pericytes regulate the blood-brain barrier. Nature 2010;468:557–61.
27. Daneman R, Zhou L, Kebede AA, Barres BA. Pericytes are required for blood-brain barrier integrity during embryogenesis. Nature 2010;468: 562–6.
28. Dawood S, Ueno NT, Valero V, Andreopoulou E, Hsu L, Lara J, et al. Incidence of and survival following brain metastases among women with inflammatory breast cancer. Ann Oncol 2010;21:2348–55.
29. Lin NU, Eierman W, Greil R, Campone M, Kaufman B, Steplewski K, et al. Randomized phase II study of lapatinib plus capecitabine or lapatinib plus topotecan for patients with HER2-positive breast cancer brain metastases. J Neurooncol 2011;105:613–20.
30. Ekenel M, Hormigo AM, Peak S, Deangelis LM, Abrey LE. Capecitabine therapy of central nervous system metastases from breast cancer. J Neurooncol 2007;85:223–7.
31. Freedman RA, Bullitt E, Sun L, Gelman R, Harris G, Ligibel JA, et al. A phase II study of sagopilone (ZK 219477; ZK-EPO) in patients with breast cancer and brain metastases. Clin Breast Cancer 2011;11: 376–83.
32. Abrey LE, Olson JD, Raizer JJ, Mack M, Rodavitch A, Boutros DY, et al. A phase II trial of temozolomide for patients with recurrent or progressive brain metastases. J Neurooncol 2001;53:259–65.
33. Sarin H, Kanevsky AS, Wu H, Sousa AA, Wilson CM, Aronova MA, et al. Physiologic upper limit of pore size in the blood-tumor barrier of malignant solid tumors. J Transl Med 2009;7:51.
34. Connell JJ, Chatain G, Cornelissen B, Vallis KA, Hamilton A, Seymour L, et al. Selective permeabilization of the blood-brain barrier at sites of metastasis. J Natl Cancer Inst 2013;105:1634–43.
35. Avraham HK, Jiang S, Fu Y, Nakshatri H, Ovadia H, Avraham S. Angiopoietin-2 mediates blood-brain barrier impairment and colonization of triple-negative breast cancer cells in brain. J Pathol 2014; 232:369–81.
36. Raza A, Franklin MJ, Dudek AZ. Pericytes and vessel maturation during tumor angiogenesis and metastasis. Am J Hematol 2010;85: 593–8.
37. Cooke VG, LeBleu VS, Keskin D, Khan Z, O'Connell JT, Teng Y, et al. Pericyte depletion results in hypoxia-associated epithelial-to-mesenchymal transition and metastasis mediated by met signaling pathway. Cancer Cell 2012;21:66–81.
38. Xian X, Hakansson J, Stahlberg A, Lindblom P, Betsholtz C, Gerhardt H, et al. Pericytes limit tumor cell metastasis. J Clin Invest 2006;116:642–51.
39. Winkler EA, Bell RD, Zlokovic BV. Central nervous system pericytes in health and disease. Nat Neurosci 2011;14:1398–405.
40. Goritz C, Dias DO, Tomilin N, Barbacid M, Shupliakov O, Frisen J. A pericyte origin of spinal cord scar tissue. Science 2011;333:238–42.
41. Kalluri R, Weinberg RA. The basics of epithelial-mesenchymal transition. J Clin Invest 2009;119:1420–8.
42. Yao Y, Chen ZL, Norris EH, Strickland S. Astrocytic laminin regulates pericyte differentiation and maintains blood brain barrier integrity. Nat Commun 2014;5:3413.